

Searching for a Heavy Neutral CP-Even Higgs Boson in the BLSSM at the LHC Run 3 and HL-LHC

M. Ashry^{1,a}, S. Khalil^{2,b} and S. Moretti^{3,4,c}

¹*Department of Mathematics, Faculty of Science, Cairo University, Giza 12613, Egypt*

²*Center for Fundamental Physics, Zewail City of Science
and Technology, 6th of October City, Giza 12578, Egypt*

³*School of Physics and Astronomy, University of Southampton, Highfield, Southampton SO17 1BJ, UK*

⁴*Department of Physics & Astronomy, Uppsala University, Box 516, SE-751 20 Uppsala, Sweden*

The detection of a heavy neutral CP-even Higgs boson of the $B - L$ Supersymmetric Standard Model (BLSSM), h' , with $m_{h'} \simeq 400$ GeV, at the Large Hadron Collider (LHC) for a center-of-mass energy of $\sqrt{s} = 14$ TeV, is investigated. The following production and decay channels are considered: $gg \rightarrow h' \rightarrow ZZ \rightarrow 4\ell$ and $gg \rightarrow h' \rightarrow W^+W^- \rightarrow 2\ell + \cancel{E}_T$ (with \cancel{E}_T being the Missing Transverse Energy (MET)), where $\ell = e, \mu$, with integrated luminosity $L_{\text{int}} = 300 \text{ fb}^{-1}$ (Run 3). Furthermore, we also look into the di-Higgs channel $gg \rightarrow h' \rightarrow hh \rightarrow b\bar{b}\gamma\gamma$ at the High-Luminosity LHC (HL-LHC) with an integrated luminosity of $L_{\text{int}} = 3000 \text{ fb}^{-1}$. We demonstrate that promising signals with high statistical significance can be obtained through the three aforementioned channels.

I. INTRODUCTION

The search for a heavy neutral CP-even Higgs boson at the current Run 3 of the LHC and a future HL-LHC is an active area of research [1–9]. This is so because virtually any extension of the Higgs sector beyond the single doublet structure of the Standard Model (SM), in which the only neutral CP-even state of it is identified with the particle that was discovered in 2012 at the LHC by the ATLAS and CMS experiments [10, 11], contains it. As a result, probing such a heavy Higgs boson is one of the main goals of the LHC experiments, as it could well provide the first hint for physics Beyond the SM (BSM). Both ATLAS and CMS have searched for a heavy Higgs boson and the corresponding analyses typically involve looking for events in which the heavy Higgs boson is produced and then decays into SM particles, such as W^\pm or Z bosons, in turn decaying into leptons or jets [1], or into the SM Higgs boson itself [12], which then decays into b quarks or τ leptons.

Supersymmetric extensions of the SM are one of the BSM frameworks that consistently predict the existence of several Higgs bosons, including a heavy neutral CP-even one. Such a Higgs boson mass can be significantly larger than the one of the SM Higgs state, potentially reaching several hundred GeV. For example, the Minimal Supersymmetric Standard Model (MSSM) contains five

^a mustafa@sci.cu.edu.eg

^b skhalil@zewailcity.edu.eg

^c s.moretti@soton.ac.uk; stefano.moretti@physics.uu.se

Higgs bosons: two CP-even (h and H , with $m_h < m_H$), one CP-odd (A) and two charged states (H^+ and H^-): for reviews, see, e.g., [13]. This is the simplest construct implementing supersymmetry, where the lightest CP-even Higgs boson, h , is designated as the SM Higgs boson, with a mass of 125 GeV, which, however, imposes a strenuous configuration on the MSSM parameter space, forcing the other CP-even Higgs boson, H , to be rather heavy and significantly decoupled. However, if supersymmetry is non-minimal, in either its gauge or Higgs sector or both, then the mass of additional CP-even Higgs states can become rather less constrained [14]. An example of this is the so-called BLSSM, which indeed offers the possibility of LHC signals for a CP-even Higgs state not only above the SM Higgs mass, e.g., in the range up to 500 GeV [9], but also afford one with a lighter mass spectrum, in turn able to explain past [15, 16] and present data anomalies [17].

The BLSSM is a theoretical extension of the MSSM that includes an additional $U(1)$ gauge symmetry known as $B - L$ (baryon number minus lepton number) [18–21] as well as an extended Higgs sector. The $B - L$ symmetry is motivated by the observation that the difference between baryon and lepton number is conserved in many particle physics processes. In the BLSSM, the $B - L$ symmetry may be broken at the few TeV scale, giving rise to new particles such as two new extra neutral CP-even Higgs bosons. One of them, labeled h' , can have energies in the hundreds of GeV range. It is indeed the presence of such a h' state that causes the aforementioned new phenomenology to emerge in collider experiments, which can then be used to test the BLSSM hypothesis.

We emphasize that the SM-like Higgs state, henceforth labeled h throughout, is derived from the real parts of the neutral components of the Electro-Weak (EW) scalar doublets H_u and H_d whereas the (typically) next-to-lightest Higgs boson, h' , stems from the real parts of the neutral components of the $B - L$ scalar singlets χ_1 and χ_2 . Despite the fact that the mass mixing between these two types of Higgs bosons is negligible, a non-vanishing kinetic mixing allows for relevant couplings between h' and the SM particles, resulting in a total cross section of h' production and decay into W^+W^- , ZZ or hh of $\mathcal{O}(1)$ fb. These signals are typically smaller than the associated backgrounds but, by using appropriate selection strategies, they can be probed with a reasonably high sensitivity. However, given that current experimental limits have significantly constrained also the BLSSM parameter space above and beyond what allowed for in Ref. [9], which targeted Run 2 sensitivities, we revisit here the scope of Run 3 and the HL-LHC in accessing the heavy neutral CP-even Higgs boson of the BLSSM, h' , in the mass region of 400 GeV or so.

The paper is organized as follows. We briefly review the BLSSM particle content, superpotential and gauge structure in Sec. II, where we also discuss at some length the Higgs sector. Studies of h' signals at the LHC are then carried out in Sec. III, wherein a detailed Monte Carlo (MC) analysis for h' production via (mostly) gluon-gluon fusion (ggF) and decay via $W^+W^- \rightarrow 2\ell + \cancel{E}_T$, $ZZ \rightarrow 4\ell$ and $hh \rightarrow b\bar{b}\gamma\gamma$ is performed. Our conclusions and final remarks are given in Sec. IV.

II. THE BLSSM

The BLSSM is based on the gauge symmetry group $SU(3)_C \times SU(2)_L \times U(1)_Y \times U(1)_{B-L}$. This model is a natural extension of the MSSM, with: i) three chiral singlet superfields \hat{N}_i introduced to cancel the $U(1)_{B-L}$ triangle anomaly and acting as right-handed neutrinos, thereby accounting for the measurements of light neutrino masses; ii) two chiral SM-singlet Higgs superfields ($\hat{\chi}_1, \hat{\chi}_2$) with $B-L$ charge = ± 2 to spontaneously break the $U(1)_{B-L}$ gauge group; iii) a vector superfield, Z' , necessary to gauge $U(1)_{B-L}$. The quantum numbers of the chiral superfields with respect to the SM gauge group ($\mathbb{G}_{\text{SM}} = SU(3)_C \otimes SU(2)_L \otimes U(1)_Y$) and $U(1)_{B-L}$ one are summarized in Table I.

Superfield	Spin-0	Spin- $\frac{1}{2}$	Generations	$\mathbb{G}_{\text{SM}} \otimes U(1)_{B-L}$
\hat{Q}	\tilde{Q}	Q	3	$(\mathbf{3}, \mathbf{2}, \frac{1}{6}, \frac{1}{6})$
\hat{d}^c	\tilde{d}^c	d^c	3	$(\bar{\mathbf{3}}, \mathbf{1}, \frac{1}{3}, -\frac{1}{6})$
\hat{u}^c	\tilde{u}^c	u^c	3	$(\bar{\mathbf{3}}, \mathbf{1}, -\frac{2}{3}, -\frac{1}{6})$
\hat{L}	\tilde{L}	L	3	$(\mathbf{1}, \mathbf{2}, -\frac{1}{2}, -\frac{1}{2})$
\hat{E}^c	\tilde{e}^c	e^c	3	$(\mathbf{1}, \mathbf{1}, 1, \frac{1}{2})$
\hat{N}^c	\tilde{N}^c	N^c	3	$(\mathbf{1}, \mathbf{1}, 0, \frac{1}{2})$
\hat{H}_d	H_d	\tilde{H}_d	1	$(\mathbf{1}, \mathbf{2}, -\frac{1}{2}, 0)$
\hat{H}_u	H_u	\tilde{H}_u	1	$(\mathbf{1}, \mathbf{2}, \frac{1}{2}, 0)$
$\hat{\chi}_1$	χ_1	$\tilde{\chi}_1$	1	$(\mathbf{1}, \mathbf{1}, 0, -1)$
$\hat{\chi}_2$	χ_2	$\tilde{\chi}_2$	1	$(\mathbf{1}, \mathbf{1}, 0, 1)$

TABLE I: Chiral superfields and their quantum numbers in the BLSSM.

The BLSSM superpotential is given by

$$W = Y_u^{ij} \hat{u}_i^c \hat{Q}_j \cdot \hat{H}_u - Y_d^{ij} \hat{d}_i^c \hat{Q}_j \cdot \hat{H}_d - Y_e^{ij} \hat{E}_i^c \hat{L}_j \cdot \hat{H}_d + Y_\nu^{ij} \hat{N}_i^c \hat{L}_j \cdot \hat{H}_u + \frac{1}{2} Y_N^{ij} \hat{N}_i^c \hat{\chi}_1 \hat{N}_j^c + \mu \hat{H}_u \cdot \hat{H}_d - \mu' \hat{\chi}_1 \hat{\chi}_2. \quad (1)$$

The relevant soft supersymmetry-breaking terms, adopting the usual universality assumptions at the Grand Unification Theory (GUT) scale, are given by

$$-\mathcal{L}_{\text{soft}} = m_0^2 \sum_{\phi} |\phi|^2 + Y_u^A \tilde{Q} H_2 \tilde{U}^c + Y_d^A \tilde{Q} H_1 \tilde{D}^c + Y_e^A \tilde{L} H_1 \tilde{E}^c + Y_\nu^A \tilde{L} H_2 \tilde{\nu}^c + Y_S^A \tilde{\nu}^c \eta_1 \tilde{S}_2 + \left[B (\mu H_1 H_2 + \mu' \eta_1 \eta_2) + \frac{1}{2} m_{1/2} \left(\tilde{g}^a \tilde{g}^a + \tilde{W}^a \tilde{W}^a + \tilde{B} \tilde{B} + \tilde{B}' \tilde{B}' \right) + h.c. \right], \quad (2)$$

where the sum in the first term runs over $\phi = \tilde{Q}, \tilde{U}, \tilde{D}, \tilde{L}, \tilde{E}, \tilde{N}, H_{1,2}, \chi_{1,2}$ and $(Y_f^A)_{ij} \equiv A_0 (Y_f)_{ij}$ ($f = u, d, e, \nu, S$) is the trilinear scalar interaction associated with the fermion Yukawa coupling. The $B-L$ symmetry can be radiatively broken by the following non-vanishing Vacuum Expectation

Values (VEVs): $\langle \chi_1 \rangle = v'_1$ and $\langle \chi_2 \rangle = v'_2$. We define $\tan \beta'$ as the ratio of these VEVs ($\tan \beta' = v'_1/v'_2$) in analogy to the MSSM case ($\tan \beta = v_2/v_1$) [18, 22].

After $B - L$ symmetry breaking, the new gauge boson, Z' , acquires its mass from the kinetic term of the $B - L$ Higgs fields, $\chi_{1,2}$. Namely, we have

$$M_{Z'}^2 = g_{BL}^2 v'^2 + \frac{1}{4} \tilde{g}^2 v^2, \quad (3)$$

where \tilde{g} is the gauge coupling mixing between $U(1)_Y$ and $U(1)_{B-L}$ and $v' = \sqrt{v_1'^2 + v_2'^2}$. Furthermore, the mixing angle between the (SM) Z and (BLSSM) Z' states is given by

$$\tan 2\theta' = \frac{2\tilde{g}\sqrt{g_1^2 + g_2^2}}{\tilde{g}^2 + 16(\frac{v'}{v})^2 g_{BL}^2 - g_2^2 - g_1^2}, \quad (4)$$

which should be $\lesssim 10^{-3}$.

We now turn to the neutral CP-even Higgs bosons in the BLSSM. The Higgs potential is

$$\begin{aligned} V(H, \chi) = & |\mu|^2 (|H_u^0|^2 + |H_d^0|^2) + |\mu'|^2 (|\chi_1|^2 + |\chi_2|^2) + \frac{g^2}{8} (|H_u^0|^2 - |H_d^0|^2)^2 + \frac{g_{BL}^2}{2} (|\chi_1|^2 - |\chi_2|^2)^2 \\ & - \frac{\tilde{g}g_{BL}}{4} (|H_u^0|^2 - |H_d^0|^2) (|\chi_1|^2 - |\chi_2|^2) - m_1^2 |\chi_1|^2 - m_2^2 |\chi_2|^2 - B_{\mu'} \chi_1 \chi_2. \end{aligned} \quad (5)$$

We expand the neutral components around their VEVs:

$$H_{u,d}^0 = \frac{1}{\sqrt{2}} (v_{u,d} + \sigma_{u,d} + i\phi_{u,d}), \quad \chi_{1,2} = \frac{1}{\sqrt{2}} (v_{1,2} + \sigma_{1,2} + i\phi_{1,2}). \quad (6)$$

The Higgs bosons (symmetric) mass matrix in the basis $(\sigma_u, \sigma_d, \sigma_1, \sigma_2)$ is given in block form

$$M_H^2 = \begin{pmatrix} M_{HH}^2 & M_{H\chi}^2 \\ \cdot & M_{\chi\chi}^2 \end{pmatrix}, \quad (7)$$

where the off-diagonal block mixing of both the MSSM and $B - L$ sectors is

$$M_{H\chi}^2 = \frac{1}{2} \tilde{g}g_{BL} \begin{pmatrix} -v_u v_1 & v_u v_2 \\ v_d v_1 & -v_d v_2 \end{pmatrix} = \frac{vx}{2} \tilde{g}g_{BL} \begin{pmatrix} -s_\beta s_{\beta'} & s_\beta c_{\beta'} \\ c_\beta s_{\beta'} & -c_\beta c_{\beta'} \end{pmatrix} \quad (8)$$

(where we have used the shorthand notations $s_X \equiv \sin X$ and $c_X \equiv \cos X$). The MSSM Higgs mass matrix M_{HH}^2 in the basis (σ_u, σ_d) is given by

$$M_{HH}^2 = \begin{pmatrix} \frac{\tilde{g}g_{BL}}{4} x^2 c_{2\beta'} + \frac{1}{8} g^2 v^2 (23s_\beta^2 - 7c_\beta^2) + \frac{B_\mu}{t_\beta} & -B_\mu - \frac{g^2}{4} v^2 s_{2\beta} \\ \cdot & -\frac{\tilde{g}g_{BL}}{4} x^2 c_{2\beta'} - \frac{1}{8} g^2 v^2 (7s_\beta^2 - 23c_\beta^2) + B_\mu t_\beta \end{pmatrix} \quad (9)$$

(where we have used the shorthand notation $t_X \equiv \tan X$) and the $B - L$ Higgs mass matrix $M_{\chi\chi}^2$ in the basis (σ_1, σ_2) is given by

$$M_{\chi\chi}^2 = \begin{pmatrix} \frac{\tilde{g}g_{BL}}{4} v^2 c_{2\beta} + \frac{1}{2} g_{BL}^2 x^2 (23s_{\beta'}^2 - 7c_{\beta'}^2) + \frac{B'_\mu}{t_{\beta'}} & -B_{\mu'} - g_{BL}^2 x^2 s_{2\beta'} \\ \cdot & -\frac{\tilde{g}g_{BL}}{4} v^2 c_{2\beta} - \frac{1}{2} g_{BL}^2 x^2 (7s_{\beta'}^2 - 23c_{\beta'}^2) + B'_\mu t_{\beta'} \end{pmatrix}, \quad (10)$$

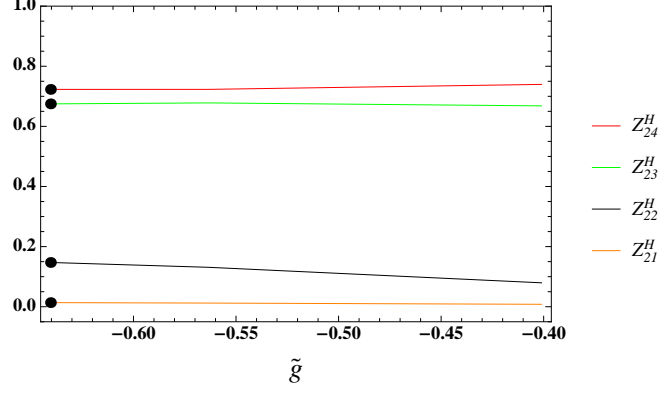


FIG. 1: The Higgs mixing Z_{2i}^H ($i = 1, \dots, 4$) versus the gauge kinetic mixing coupling \tilde{g} . The values corresponding to the Benchmark Point (BP) of (forthcoming) Table IIa are labeled by \bullet .

where the tree-level tadpole equation solutions give

$$\begin{aligned} B_\mu &= t_{2\beta} \left(-\frac{1}{8} g^2 v^2 c_{2\beta} + \frac{1}{4} g_{BL} \tilde{g} x^2 c_{2\beta'} - \frac{1}{2} (m_d^2 - m_u^2) \right), \\ B'_\mu &= t_{2\beta'} \left(-\frac{1}{2} g_{BL}^2 x^2 c_{2\beta'} + \frac{1}{4} g_{BL} \tilde{g} v^2 c_{2\beta} - \frac{1}{2} (m_2^2 - m_1^2) \right). \end{aligned} \quad (11)$$

The heavy Higgs boson tree-level mass eigenvalues are given in terms of the lightest SM-like Higgs boson $h \equiv h_1$ mass, which is fixed at $m_h = 125$ GeV, and the lightest $B - L$ Higgs boson $h' \equiv h_2$ mass, which we take to be $m_{h'} = 400$ GeV, as follows

$$m_{H,H'}^2 = \frac{1}{2} \left[T_H - m_h^2 - m_{h'}^2 \pm \sqrt{(T_H - m_h^2 - m_{h'}^2)^2 - \frac{4D_H}{m_h^2 m_{h'}^2}} \right], \quad (12)$$

where we have the determinant $D_H = \text{Det}(M_H^2)$ and the trace $T_H = \text{Tr}(M_H^2)$ is given by

$$T_H = 2|\mu|^2 + m_d^2 + m_u^2 + 2g^2 v^2 + 2|\mu'|^2 + m_2^2 + m_1^2 + 8g_{BL}^2 x^2. \quad (13)$$

For $\sigma_i = \sigma_d, \sigma_u, \sigma_1, \sigma_2$, one has $\sigma_i = Z_{ji}^H h_j$, $h_j = h, h', H, H'$ and $h_j = Z_{ij}^H \sigma_i$.

$$h' \approx Z_{22}^H \sigma_d + Z_{23}^H \sigma_1 + Z_{24}^H \sigma_2. \quad (14)$$

In Fig. 1, we display the mixing Z_{2i}^H versus the gauge kinetic mixing \tilde{g} . As can be seen from this plot, h' is essentially generated from $\sigma_{1,2}$ with smaller contributions from the real components of σ_d which connects it however to the SM sector. Table IIa presents the $B - L$ gaugino soft mass, $M_{\tilde{B}}$, and the MSSM and $B - L$ gaugino mixing soft mass, $M_{\tilde{B}\tilde{B}'}$. The MSSM gaugino soft masses (bino, wino, gluino), $M_{\tilde{B}}, M_{\tilde{W}}, M_{\tilde{g}}$, are fixed to $M_{\tilde{B}} = M_1 \sim 7.74 \times 10^2$ GeV, $M_{\tilde{W}} = M_2 \sim 8.52 \times 10^2$ GeV and $M_{\tilde{g}} = M_3 \sim 6.38 \times 10^2$ GeV, respectively.

g_{BL}	\tilde{g}	t_β	$t_{\beta'}$	v'	m_u^2	m_d^2	m_1^2	m_2^2	$M_{\tilde{B}'}$	$M_{\tilde{B}\tilde{B}'}$
0.675	-0.640	11.034	1.288	4875	-1.30×10^7	9.30×10^6	-5.75×10^5	4.02×10^6	1.49×10^3	-1.55×10^3

(a) Our BP, wherein dimensionful parameters are all in GeV.

Z_{11}^H	Z_{12}^H	Z_{13}^H	Z_{14}^H	Z_{21}^H	Z_{22}^H	Z_{23}^H	Z_{24}^H	Z_{31}^H	Z_{32}^H	Z_{33}^H	Z_{34}^H	Z_{41}^H	Z_{42}^H	Z_{43}^H	Z_{44}^H
0.089	0.987	-0.100	-0.088	0.012	0.131	0.678	0.723	0.030	0.009	0.728	-0.685	-0.995	0.091	0.021	-0.019

(b) Neutral CP-even Higgs mixing corresponding to the BP of Table IIa.

m_{H^\pm}	m_A	$m_{A'}$	$m_{h_1 \equiv h}$	$m_{h_2 \equiv h'}$	$m_{h_3 \equiv H'}$	$m_{h_4 \equiv H}$	$M_{Z'}$
4384	2587	4384	125	397	4241	4402	3300

(c) Higgs mass spectrum and $M_{Z'}$ in GeV corresponding to the BP of Table IIa.

The Higgs bosons interaction couplings with fermion and gauge bosons are

$$\Gamma_{dd}^{h_2} = -\frac{1}{\sqrt{2}} Y^d Z_{22}^H = -\frac{m_d}{v c_\beta} Z_{22}^H, \quad (15)$$

$$\Gamma_{uu}^{h_2} = -\frac{1}{\sqrt{2}} Y^u Z_{22}^H = -\frac{m_u}{v s_\beta} Z_{22}^H, \quad (16)$$

$$g_{h'W+W^-} \approx g_2 M_W s_\beta Z_{22}^H, \quad (17)$$

$$g_{h'ZZ} \approx g_{h'W+W^-} \left(\sec \theta_w - \frac{\tilde{g}}{g_2} s_{\theta_{w'}} \right)^2, \quad (18)$$

$$\begin{aligned} g_{h'hh} \approx & \frac{1}{4} Z_{22}^H \left(4\tilde{g} g_{BL} x Z_{12}^H \left(Z_{13}^H s_{\beta'} - Z_{14}^H c_{\beta'} \right) - 3g^2 v s_\beta (Z_{12}^H)^2 \right) \\ & + \frac{1}{2} Z_{23}^H \left(2g_{BL}^2 x \left(3s_{\beta'} (Z_{13}^H)^2 - 2c_{\beta'} Z_{13}^H Z_{14}^H - s_{\beta'} (Z_{14}^H)^2 \right) - \tilde{g} g_{BL} \left(x s_{\beta'} (Z_{12}^H)^2 + 2v s_\beta Z_{12}^H Z_{13}^H \right) \right) \\ & + \frac{1}{2} Z_{24}^H \left(2g_{BL}^2 x \left(c_{\beta'} (Z_{13}^H)^2 + 2s_{\beta'} Z_{13}^H Z_{14}^H - 3c_{\beta'} (Z_{14}^H)^2 \right) \right), \end{aligned} \quad (19)$$

where θ_w and $\theta_{w'}$ are the weak and $Z - Z'$ mixing angles, respectively. For $t_{\beta'} \sim 1$, $Z_{12}^H \sim 1$, $Z_{13}^H, Z_{14}^H \ll 1$, $Z_{23}^H, Z_{24}^H \sim \frac{1}{\sqrt{2}}$, the trilinear Higgs boson coupling $h'hh$ (relevant to our forthcoming analysis) is approximated by

$$\begin{aligned} g_{h'hh} \approx & -\frac{1}{2} (Z_{12}^H)^2 \left(\frac{3}{2} g^2 v s_\beta Z_{22}^H + \tilde{g} g_{BL} x (s_{\beta'} Z_{23}^H + c_{\beta'} Z_{24}^H) \right) \\ \sim & -\frac{1}{2} \left(\frac{3}{2} g^2 v s_\beta Z_{22}^H + \frac{1}{\sqrt{2}} \tilde{g} g_{BL} x (s_{\beta'} + c_{\beta'}) \right) \\ \sim & -\frac{1}{2} \left(\frac{3}{2} g^2 v s_\beta Z_{22}^H + \tilde{g} g_{BL} x \right). \end{aligned} \quad (20)$$

We notice, from Eq. (20), that setting the gauge kinetic mixing coupling $\tilde{g} \equiv 0$ reduces the $g_{h'hh}$ coupling.

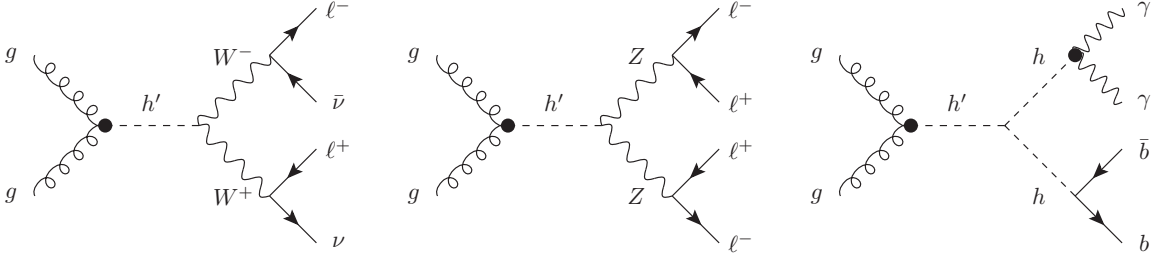


FIG. 2: Feynman diagrams for h' production via ggF and decays via (from left to right) $W^+W^- \rightarrow 2\ell + \cancel{E}_T$, $h' \rightarrow ZZ \rightarrow 4\ell$ and $h' \rightarrow hh \rightarrow b\bar{b}\gamma\gamma$.

III. SEARCH FOR A HEAVY NEUTRAL CP-EVEN HIGGS BOSON AT THE LHC

Many computational tools are used throughout this work, from building the model analytically to performing the numerical simulations at detector level. The BLSSM was first implemented into the SARAH package for Mathematica and the output was then passed to SPHENO [23, 24] for numerical calculations of the particle spectrum. After that, the ensuing UFO model was used in MADGRAPH [25] for MC event generation and Matrix Element (ME) calculations. After that, PYTHIA was used to simulate initial and final state radiation (through the Parton Shower (PS) formalism) as well as fragmentation/hadronization effects [26]. For detector simulation, the PYTHIA output was passed to DELPHES [27]. Finally, for data analysis, we used MADANALYSIS [28]. As for the BP used, we made sure that it was consistent with HIGGSBOUNDS and HIGGSSIGNALS [29, 30] limits, as obtained from the latest LHC data.

The Feynman diagrams associated to the h' production and decay mechanisms discussed here are found in Fig. 2, wherein the \bullet symbol is meant to signify the exact loop function allowing for both b and t quark contributions. The Higgs production and decay rates are computed by factorising the h' propagator, so that the overall event yield can be broken down into the h' production cross section and decay Branching Ratios (BRs). The MC event generation is done at Leading Order (LO) for both Signal (S) and Background (B), however, we include Next-to-Next-to-LO (NNLO) inclusive k -factors from Quantum Chromo-Dynamics (QCD) in computing our significances, specifically, we use 2.2 for the ggF signal and 1.2 for the Vector Boson Fusion (VBF) one (see below) as well as the (EW) backgrounds [31–35]. The cross section for ggF, properly convoluted with the default Parton Distribution Functions (PDFs) of our ME generator (namely, $\sigma(pp \rightarrow h')$), as function of \tilde{g} , is found in Fig. 3 (left), for $\sqrt{s} = 14$ TeV. In Fig. 3 (right) we show instead the h' decay BRs, again, as functions of \tilde{g} . In both such plots, the symbol \bullet refers to the BP adopted here, for which the corresponding σ and BR values are found in Table III. The production cross section of h' depends significantly on \tilde{g} , which is (as mentioned) the only source of mixing

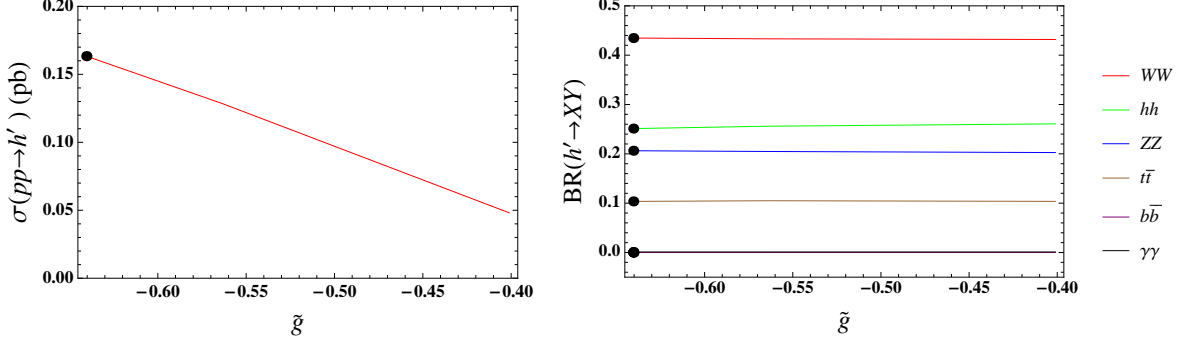


FIG. 3: ggF h' production cross section at $\sqrt{s} = 14$ TeV (left) and h' decay BRs (right) versus the kinetic mixing coupling \tilde{g} . The values corresponding to the BP of Table IIa are labeled by \bullet .

between the BLSSM Higgs $\chi_{1,2}$ and the MSSM Higgs doublets $H_{u,d}$ that enables h' couplings with SM particles. However, the h' decay BRs are not significantly affected by it because both the partial and total decay widths of h' in each channel receive nearly the same contribution from \tilde{g} , which cancels out from the BRs. It is noteworthy that the three most significant decay channels are the bosonic ones in W^+W^- , ZZ and hh . In contrast, the fermionic decay channels into $t\bar{t}$ and $b\bar{b}$ are relatively less significant. Therefore, in the forthcoming MC analysis, we will concentrate on the former three decay channels.

For each channel, there are many corresponding background processes and all can be reduced by applying the cut-flows of Tables IVa, IVb and IVc, in correspondence of the three aforementioned channels, respectively. What remain in all cases, though, are the irreducible backgrounds $pp \rightarrow 2\ell + \cancel{E}_T$, $pp \rightarrow 4\ell$ and $pp \rightarrow \gamma\gamma b\bar{b}$.

The following standard acceptance cuts on transverse momentum (P_T), pseudorapidity (η) and angular separation (ΔR) of the final state leptons, jets and photons are applied:

1. $(P_T)_j \geq 20$, $(P_T)_a \geq 10$, $a = \gamma, \ell$,
2. $|\eta_j| \leq 5$, $|\eta_a| \leq 2.5$, $a = \gamma, \ell$,
3. $\Delta R_{ab} \geq 0.4$, $a, b = j, \gamma, \ell$.

In Tables IVa, IVb and IVc, the kinematical variables are defined such that M_{eff} is the effective mass being obtained as the sum of the transverse momentum of all final state objects and the transverse energy, and E_T is the scalar sum of the transverse energy of all (visible) final state objects in the plane transverse to the beam [28]. Furthermore, $M_{ab\dots}$ is an invariant mass and ΔR_{ab} is the separation between final state objects. (Note that an (opposite-sign) di-lepton mass reconstruction around one M_Z value in the 4ℓ channel is not useful, as the irreducible background is here dominated by $pp \rightarrow ZZ, Z\gamma^* \rightarrow 4\ell$.)

Quantity	Value
$\text{BR}(h' \rightarrow W^+W^-)$	0.432
$\text{BR}(h' \rightarrow ZZ)$	0.203
$\text{BR}(h' \rightarrow hh)$	0.261
$\sigma(pp \rightarrow h')$	163.400 (fb)
$\sigma(pp \rightarrow h' \rightarrow W^+W^- \rightarrow 2\ell + \cancel{E}_T)$	9.256 (fb)
$\sigma(pp \rightarrow h' \rightarrow ZZ \rightarrow 4\ell)$	0.406 (fb)
$\sigma(pp \rightarrow h' \rightarrow hh \rightarrow \bar{b}b\gamma\gamma)$	0.124 (fb)

TABLE III: Production cross section σ (at $\sqrt{s} = 14$ TeV) and decay BRs into W^+W^- , ZZ and hh for the h' state (with $m_{h'} = 400$ GeV) of our BP, including the overall rates in the three final states $2\ell + \cancel{E}_T$, 4ℓ and $\bar{b}b\gamma\gamma$. Normalization is to LO for all σ 's.

A. THE $h' \rightarrow W^+W^- \rightarrow 2\ell + \cancel{E}_T$ CHANNEL

Table IVa provides the cut-flow for the h' production and decay analysis via the $2\ell + \cancel{E}_T$ signature, while event shapes and rates (the latter in correspondence to Run 3 luminosity) for

$$\sigma(pp \rightarrow h' \rightarrow W^+W^- \rightarrow 2\ell + \cancel{E}_T) \approx \sigma(pp \rightarrow h') \times \text{BR}(h' \rightarrow W^+W^- \rightarrow 2\ell + \cancel{E}_T) \quad (21)$$

are presented in Fig. 4. Herein, we also present the contributions of an additional signal channel, induced by (W^+W^- dominated) VBF with two additional (untagged) forward/backward jets, as it contributes not negligibly to the same ggF signal regions (so that it has been taken into account in extracting our final sensitivities). In this figure, the normalized (to 1) distributions used for the cut-flow (i.e., E_T , M_{eff} and $\Delta R_{\ell+\ell-}$) are presented, alongside the full transverse mass ($M_{T_{\ell+\ell-}}$) of the final state (i.e., using both leptons in its definition), the latter integrating to the actual event numbers for Run 3 and also in presence of the background contribution. Altogether, from this last spectrum, it is clear that a high signal significance can be reached, however, it also shows that the shape does not promptly correlate to the h' mass value. Yet, the significant excess seen in this channel will clearly motivate a parallel search in the 4ℓ final state, which we are illustrating next.

B. THE $h' \rightarrow ZZ \rightarrow 4\ell$ CHANNEL

Table IVb provides the cut-flow for h' production and decay via the 4ℓ channel, while some relevant kinematics, in terms of event shapes and rates (the latter, again, in correspondence to Run 3 luminosity) for

$$\sigma(pp \rightarrow h' \rightarrow ZZ \rightarrow 4\ell) \approx \sigma(pp \rightarrow h') \times \text{BR}(h' \rightarrow ZZ \rightarrow 4\ell) \quad (22)$$

is presented in Fig. 5. Here, we concentrate on the normalized (to 1) distributions in transverse energy of all leptons (E_T) and opposite-sign di-lepton invariant mass ($M_{\ell+\ell-}$), both of which

Cuts (select)	S	B	S/\sqrt{B}
Initial (no cut)	6108	720000	7.20
$E_T > 700$ GeV	703.1 ± 24.9	2219.9 ± 47.0	14.92 ± 0.008
$M_{\text{eff}} > 100$ GeV	693.1 ± 24.8	2118.5 ± 46.2	15.06 ± 0.008
$\Delta R_{\ell^+\ell^-} > 1.5$	628.2 ± 23.7	1568.3 ± 39.6	15.86 ± 0.009

(a) $pp \rightarrow h' \rightarrow W^+W^- \rightarrow 2\ell + \cancel{E}_T$ cut-flow at $L_{\text{int}} = 300 \text{ fb}^{-1}$.

Cuts (select)	S	B	S/\sqrt{B}
Initial (no cut)	267	9712	2.72
$E_T > 300$ GeV	208.75 ± 6.79	1680.2 ± 37.30	5.09 ± 0.004
$M_{\ell^+\ell^-} < 150$ GeV	173.04 ± 7.83	1414.9 ± 34.80	4.60 ± 0.005
$M_{\ell^+\ell^-} > 50$ GeV	172.80 ± 7.83	1394.7 ± 34.60	4.63 ± 0.005

(b) $pp \rightarrow h' \rightarrow ZZ \rightarrow 4\ell$ cut-flow at $L_{\text{int}} = 300 \text{ fb}^{-1}$.

Cuts (select)	S	B	S/\sqrt{B}
Initial (no cut)	951	19951560	0.213
$E_T > 200$ GeV	933.18 ± 4.19	1476867.0 ± 1169.0	$0.768 \pm 2.88 \times 10^{-6}$
$M_{\gamma\gamma} > 120$ GeV	475.50 ± 15.40	165131.0 ± 404.0	$1.170 \pm 9.31 \times 10^{-5}$
$M_{\gamma\gamma} < 135$ GeV	474.80 ± 15.40	29023.0 ± 170.0	$2.787 \pm 5.23 \times 10^{-4}$
$M_{bb} > 50$ GeV	145.50 ± 11.10	3582.7 ± 59.9	$2.431 \pm 2.93 \times 10^{-3}$
$M_{bb} < 160$ GeV	134.70 ± 10.80	1944.9 ± 44.1	$3.055 \pm 5.03 \times 10^{-3}$
$\Delta R_{\gamma\gamma} < 3.5$	133.90 ± 10.7	1824.5 ± 42.7	$3.135 \pm 5.32 \times 10^{-3}$
$\Delta R_{b\bar{b}} < 3.5$	131.90 ± 10.7	1746.2 ± 41.8	$3.156 \pm 5.50 \times 10^{-3}$
$M_{\gamma\gamma b\bar{b}} > 360$ GeV	102.71 ± 9.57	686.4 ± 26.2	$3.920 \pm 1.14 \times 10^{-2}$
$M_{\gamma\gamma b\bar{b}} < 450$ GeV	98.5 ± 9.40	403.4 ± 20.1	$4.903 \pm 1.70 \times 10^{-2}$

(c) $pp \rightarrow h' \rightarrow hh \rightarrow b\bar{b}\gamma\gamma$ cut-flow at $L_{\text{int}} = 3000 \text{ fb}^{-1}$.

TABLE IV: S vs B rates for the three signals pursued in our analysis in correspondence of our BP: the $2\ell + \cancel{E}_T$ (a), 4ℓ and $b\bar{b}\gamma\gamma$ (c) final state. We adopt here $\sqrt{s} = 14$ TeV and integrated luminosity of Run 3 and HL-LHC. Inclusive NNLO k -factors from QCD are used here throughout.

are used in our cut-flow. (Regarding the latter, notice that the loss of significance in applying the cut in invariant mass against the dominant irreducible background $pp \rightarrow ZZ, Z\gamma^* \rightarrow 4\ell$ is rather insignificant against the benefits of rejecting the irreducible one, e.g., from top-antitop quark production and fully leptonic W^+W^- decays (which has typically a harder distribution in this variable), so that the whole of the latter can be neglected.) In the end, the spectrum from which to extract the h' resonance, i.e., the final state invariant mass, $M_{4\ell}$, clearly reveals a broad excess over a 400 GeV or so mass interval, altogether yielding significances in the discovery range. In fact, also a noticeable peak appear for $M_{4\ell} \approx 400$ GeV (which, as mentioned, can be correlated

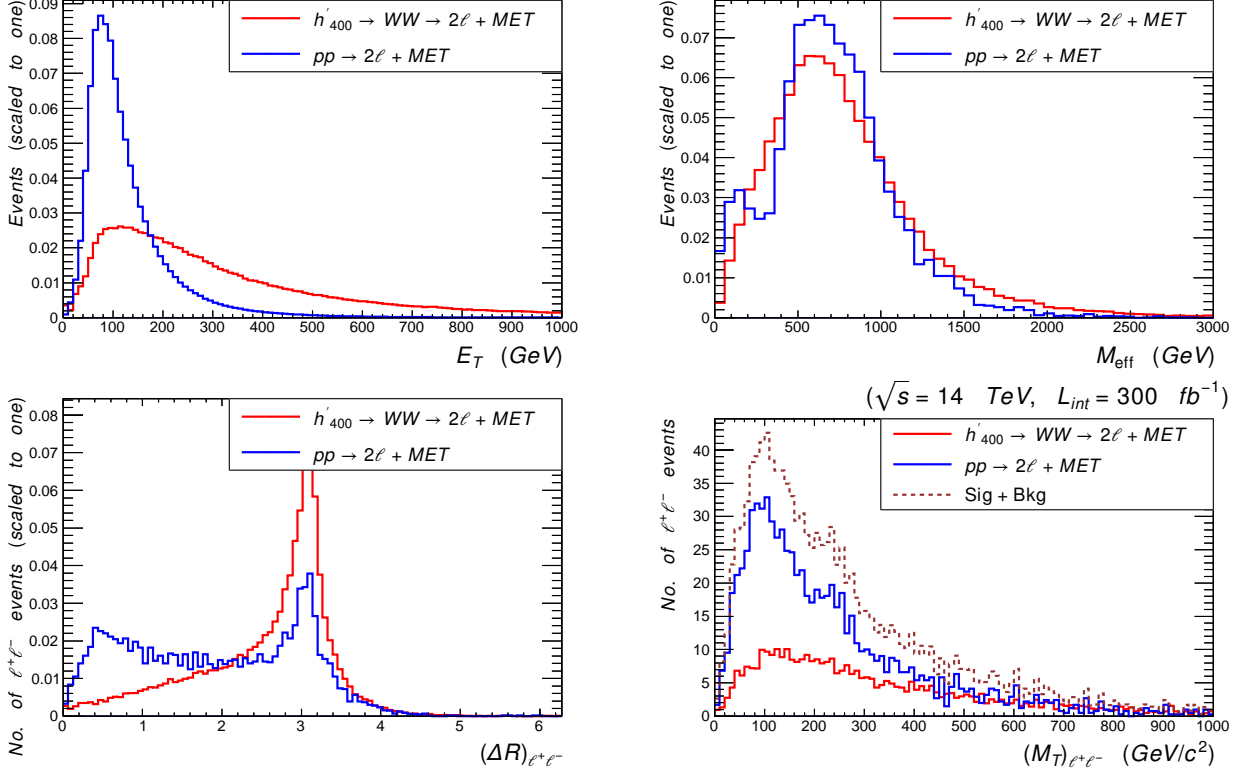


FIG. 4: S and B distributions in E_T (top-left), M_{eff} (top-right), $\Delta R_{\ell+\ell^-}$ (bottom-left) and $M_{T_{\ell+\ell^-}}$ (bottom-right), as defined in the text, the former three given before the cut-flow and normalized to 1 while the latter one given after it and normalized to the total event rate for the integrated luminosity $L_{\text{int}} = 300 \text{ fb}^{-1}$. In all cases we show both the ggF contribution to the signal $2\ell + \cancel{E}_T$ (red) for our BP and the background (blue) while for the last spectrum we also show the (stacked) distribution as well.

with the $M_{T_{\ell+\ell^-}}$ distribution in the $2\ell + \cancel{E}_T$ final state), so that one can improve further the potential for h' discovery in the 4ℓ channel by optimizing a cut in this variable.

C. THE $h' \rightarrow hh \rightarrow b\bar{b}\gamma\gamma$ CHANNEL

Table IVc provides the cut-flow for the h' production and decay analysis of the last channel we study,

$$\sigma(pp \rightarrow h' \rightarrow hh \rightarrow b\bar{b}\gamma\gamma) \approx \sigma(pp \rightarrow h') \times \text{BR}(h' \rightarrow hh \rightarrow b\bar{b}\gamma\gamma), \quad (23)$$

wherein we use HL-LHC luminosity, as this channel is not accessible during Run 3. The distributions used to inform our cut-flow herein (normalized to 1) are found in Fig. 6. These are the spectra in the transverse energy of the $b\bar{b}\gamma\gamma$ final state (E_T), $\gamma\gamma$ and $b\bar{b}$ invariant masses ($M_{\gamma\gamma}$ and $M_{b\bar{b}}$,

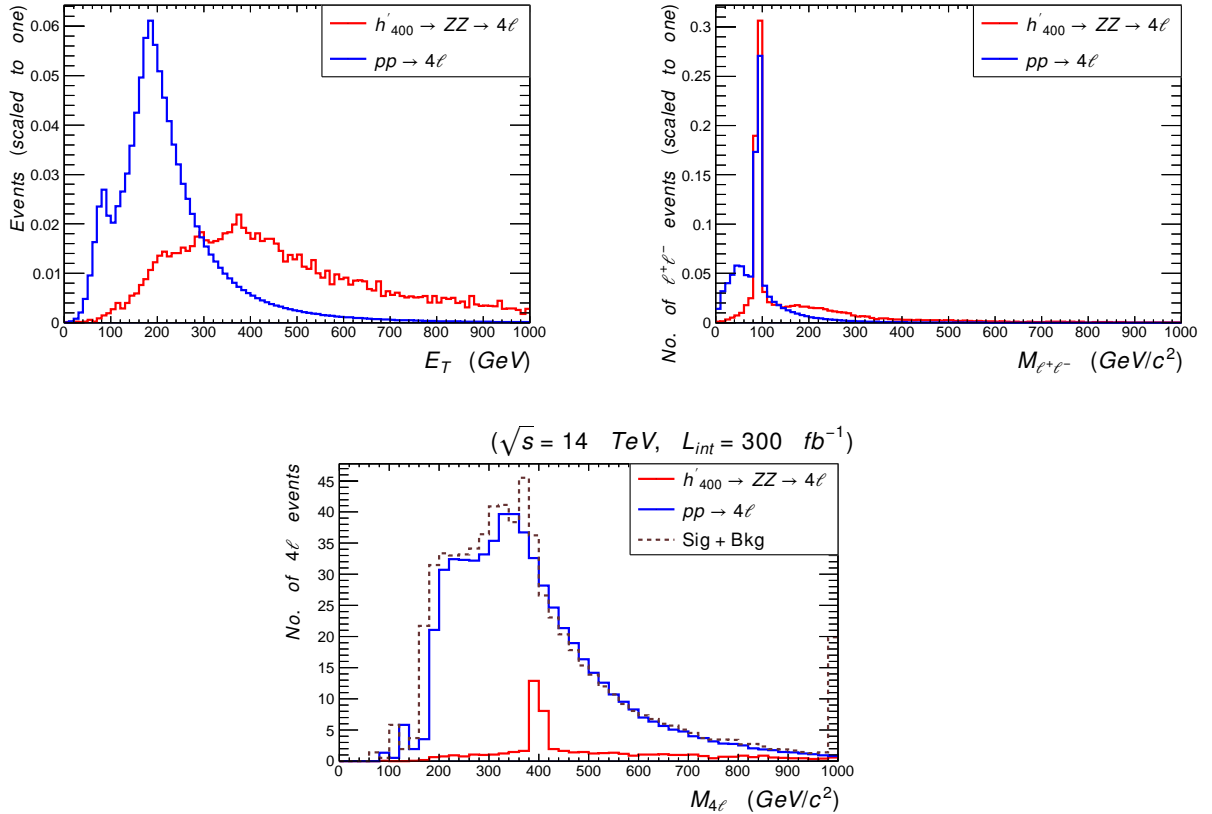


FIG. 5: S and B distributions in E_T (top-left), $M_{\ell^+\ell^-}$ (top-right) and $M_{4\ell}$ (bottom), as defined in the text, the former two given before the cut-flow and normalized to 1 while the latter one given after it and normalized to the total event rate for the integrated luminosity $L_{\text{int}} = 300 \text{ fb}^{-1}$. In all cases we show only the ggF contribution to the 4ℓ signal for our BP while for the last spectrum we also show the (stacked) distribution.

respectively) and separations ($\Delta R_{\gamma\gamma}$ and $\Delta R_{b\bar{b}}$, respectively). Such a figure also presents the invariant mass of the final state ($M_{\gamma\gamma b\bar{b}}$), normalized to the HL-LHC luminosity. As seen from the signal and background responses to the cut-flow, it is clear that knowledge of the $m_{h'}$ value, gained during Run 3 of the LHC by exploiting the two previous signatures, is crucial in accessing this signal, which can ultimately be done at the 5σ level, despite the initially overwhelming background.

D. Historical Significances

Before closing this section, we describe the patterns of significances in the three channels that we have studied, as they would evolve with luminosity, assuming fixed energy at $\sqrt{s} = 14 \text{ TeV}$. These are shown in Fig. 7. It is evident that a full characterization of the h' state, involving its coupling to SM (massive) gauge and Higgs bosons is only possible through a combined effort of

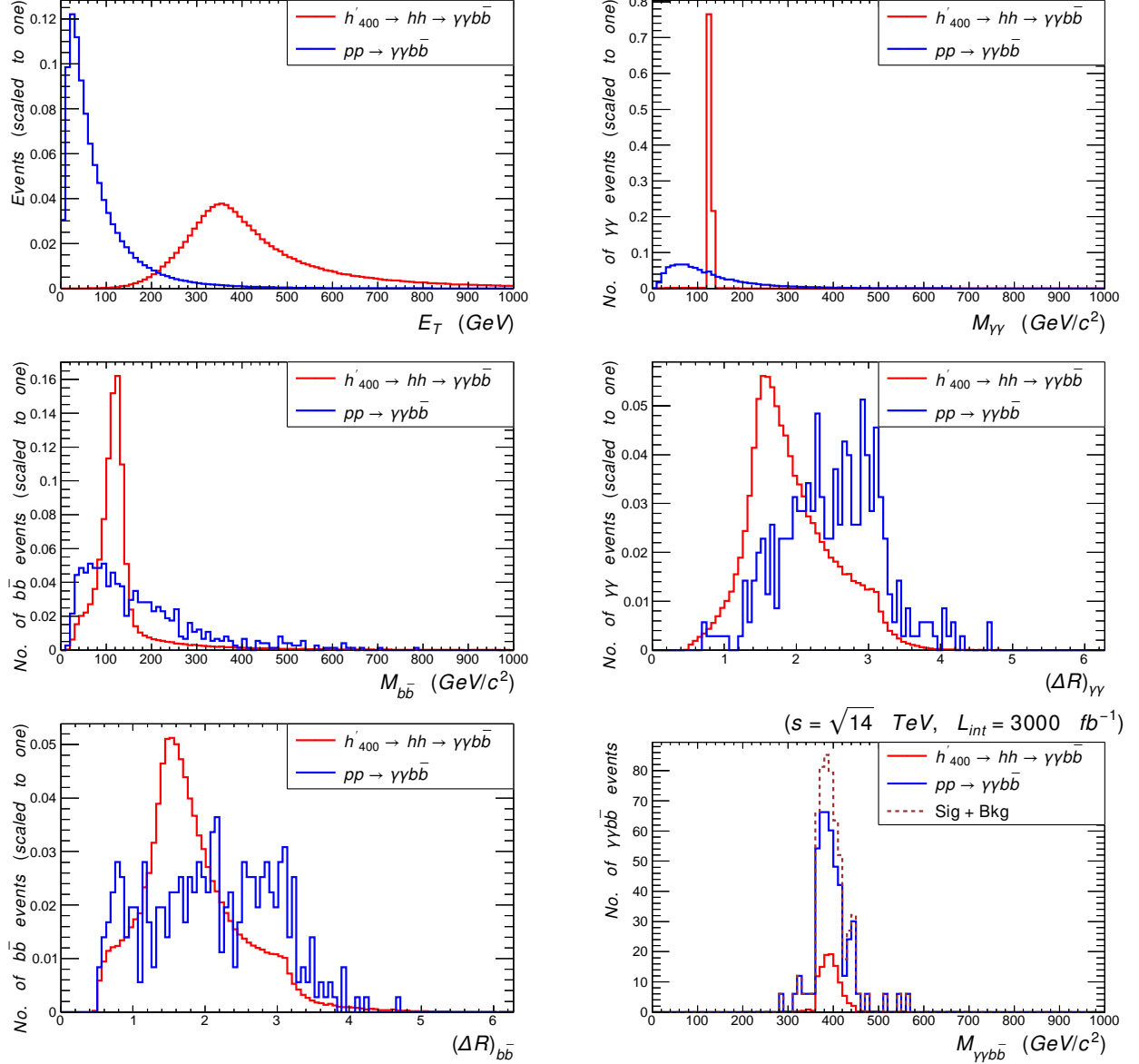


FIG. 6: S and B distributions in E_T (top-left), $M_{\gamma\gamma}$ (top-right), $M_{b\bar{b}}$ (middle-left), $\Delta R_{\gamma\gamma}$ (middle-right) $\Delta R_{b\bar{b}}$ (bottom-left) and $M_{\gamma\gamma b\bar{b}}$ (bottom-right), as defined in the text, the former 5 given before the cut-flow and normalized to 1 while the latter one given after it and normalized to the total event rate for the integrated luminosity $L_{\text{int}} = 3000 \text{ fb}^{-1}$. In all cases we show only the ggF contribution to the $b\bar{b}\gamma\gamma$ signal for our BP while for the last spectrum we also show the (stacked) distribution.

analyses to be entertained at both Run 3 of the LHC and HL-LHC.

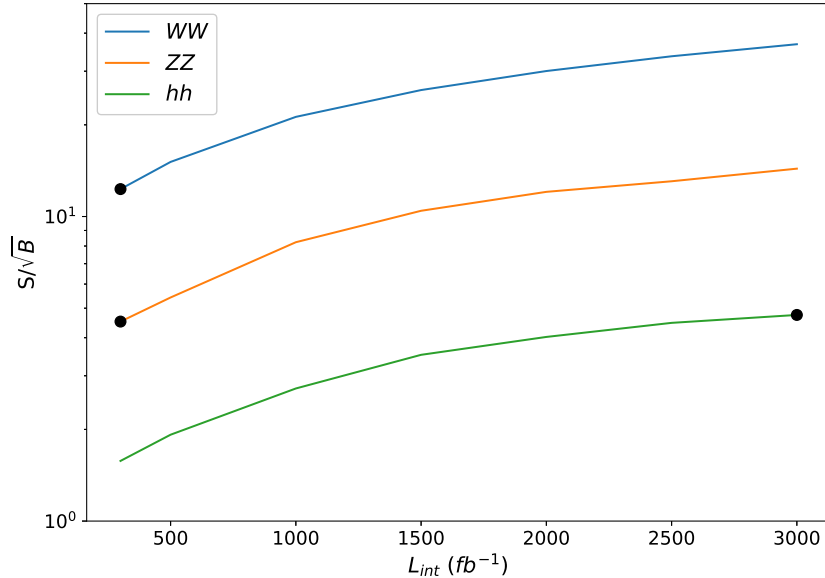


FIG. 7: Significance of the $h' \rightarrow W^+W^-, ZZ$ and hh signals that we have studied versus L_{int} for our BP. Data are produced at a center-of-mass energy of $\sqrt{s} = 14$ TeV. The rates are computed after applying the relevant kinematical analyses described in the text. The three \bullet points indicate the luminosity choices used in the MC simulations performed.

IV. CONCLUSIONS

In summary, we have shown that a theoretically well-motivated realization of supersymmetry, the so-called BLSSM, may yield detectable signals of a heavy neutral CP-even Higgs boson at the LHC, both during Run 3 and the HL-LHC phase. These emerge from the lightest (neutral) Higgs state of this scenario with prevalent $B - L$ composition, h' , while the lightest (neutral) Higgs state with predominant MSSM nature is identified with the discovered one, h (with $m_h = 125$ GeV). The subprocesses pursued to this effect, assuming a BP with an illustrative mass $m_{h'} = 400$ GeV, have been $gg \rightarrow h' \rightarrow W^+W^- \rightarrow 2\ell + \cancel{E}_T$, $gg \rightarrow h' \rightarrow ZZ \rightarrow 4\ell$ and $gg \rightarrow h' \rightarrow hh \rightarrow b\bar{b}\gamma\gamma$. The first one would be accessible during the early stages of Run 3 and the study of mass distributions would allow one to extract an indication of the h' mass. This information can then be used to optimize the selection of the second signal, which would reveal a clear pick centered around $m_{h'}$ by the end of Run 3. With the latter information available, one would then be able to establish the third signal at the HL-LHC. All this will therefore enable one to fully characterize the h' state, not only through its mass, but also in terms of its couplings, as the W^+W^- , ZZ and hh decays are the dominant ones in the BLSSM while those to $t\bar{t}$ and $b\bar{b}$ pairs may be accessible at production level through the ggF channel. This finally opens up the possibility of eventually separating the BLSSM hypothesis from

alternative ones also based on supersymmetry, since – thanks to the peculiar feature of (gauge) kinetic mixing appearing in the BLSSM (which incorporates an additional $U(1)_{B-L}$ group beyond the SM gauge symmetries) – competing signals stemming from, e.g., the MSSM would have rather different mass and coupling patterns.

We have come to these conclusions by performing a full MC analysis in presence of ME, PS, fragmentation/hadronization effects as well as detector modeling and upon devising dedicated cut-and-count cut-flows for each signature pursued. We are therefore confident that ATLAS and CMS would have sensitivity to this specific non-minimal realization of supersymmetry and advocate dedicated searches for the aforementioned signals.

ACKNOWLEDGEMENTS

The work of M.A. is partially supported by the Science, Technology & Innovation Funding Authority (STDF) under Grant No. 33495. The work of and S.K. is partially supported by STDF under Grant No. 37272. S.M. is supported in part through the NExT Institute and the Science & Technology Facilities Council (STFC) Consolidated Grant No. ST/L000296/1.

-
- [1] ATLAS-Collaboration (ATLAS) (2022), 2211.02617.
 - [2] ATLAS-Collaboration (ATLAS) (2022), 2211.01136.
 - [3] CMS-Collaboration (CMS) (2022), 2210.00043.
 - [4] A. Adhikary, B. Bhattacharjee, R. M. Godbole, N. Khan, and S. Kulkarni, *JHEP* **04**, 284 (2021), 2002.07137.
 - [5] X. Chen, Y. Xu, Y. Wu, Y.-P. Kuang, Q. Wang, H. Chen, S.-C. Hsu, Z. Hu, and C. Li, *Phys. Lett. B* **804**, 135358 (2020), 1905.05421.
 - [6] H. Bahl, P. Bechtle, S. Heinemeyer, S. Liebler, T. Stefaniak, and G. Weiglein, *Eur. Phys. J. C* **80**, 916 (2020), 2005.14536.
 - [7] J. Gu, H. Li, Z. Liu, S. Su, and W. Su, *JHEP* **12**, 153 (2017), 1709.06103.
 - [8] S. Banerjee, M. Mitra, and M. Spannowsky, *Phys. Rev. D* **92**, 055013 (2015), 1506.06415.
 - [9] A. Hammad, S. Khalil, and S. Moretti, *Phys. Rev. D* **93**, 115035 (2016), 1601.07934.
 - [10] G. Aad et al. (ATLAS), *Phys. Lett. B* **716**, 1 (2012), 1207.7214.
 - [11] S. Chatrchyan et al. (CMS), *Phys. Lett. B* **716**, 30 (2012), 1207.7235.
 - [12] N. Chernyavskaya, in *55th Rencontres de Moriond on Electroweak Interactions and Unified Theories* (2023), 2302.12631.
 - [13] A. Djouadi, *Phys. Rept.* **459**, 1 (2008), hep-ph/0503173.
 - [14] S. Moretti and S. Khalil, *Supersymmetry Beyond Minimality: From Theory to Experiment* (CRC Press, 2019), ISBN 978-0-367-87662-3.
 - [15] A. Hammad, S. Khalil, and S. Moretti, *Phys. Rev. D* **92**, 095008 (2015), 1503.05408.
 - [16] W. Abdallah, S. Khalil, and S. Moretti, *Phys. Rev. D* **91**, 014001 (2015), 1409.7837.
 - [17] A. A. Abdelalim, B. Das, S. Khalil, and S. Moretti, *Nucl. Phys. B* **985**, 116013 (2022), 2012.04952.

- [18] S. Khalil and A. Masiero, *Phys. Lett. B* **665**, 374 (2008), 0710.3525.
- [19] B. O’Leary, W. Porod, and F. Staub, *JHEP* **05**, 042 (2012), 1112.4600.
- [20] L. Basso, Ph.D. thesis, Southampton U. (2011), 1106.4462.
- [21] L. Basso, *Adv. High Energy Phys.* **2015**, 980687 (2015), 1504.05328.
- [22] S. Khalil, *Phys. Rev. D* **94**, 075003 (2016), 1606.09292.
- [23] F. Staub, *Comput. Phys. Commun.* **185**, 1773 (2014).
- [24] W. Porod and F. Staub, *Comput. Phys. Commun.* **183**, 2458 (2012).
- [25] J. Alwall, M. Herquet, F. Maltoni, O. Mattelaer, and T. Stelzer, *JHEP* **06**, 128 (2011).
- [26] T. Sjostrand, S. Mrenna, and P. Z. Skands, *Comput. Phys. Commun.* **178**, 852 (2008).
- [27] J. de Favereau, C. Delaere, P. Demin, A. Giammanco, V. Lemaître, A. Mertens, and M. Selvaggi (DELPHES 3), *JHEP* **02**, 057 (2014).
- [28] E. Conte, B. Fuks, and G. Serret, *Comput. Phys. Commun.* **184**, 222 (2013).
- [29] P. Bechtle, O. Brein, S. Heinemeyer, O. Stål, T. Stefaniak, G. Weiglein, and K. E. Williams, *Eur. Phys. J. C* **74**, 2693 (2014).
- [30] P. Bechtle, S. Heinemeyer, O. Stål, T. Stefaniak, and G. Weiglein, *Eur. Phys. J. C* **74**, 2711 (2014).
- [31] R. V. Harlander and W. B. Kilgore, *eConf C010630*, P506 (2001), hep-ph/0110200.
- [32] R. V. Harlander and W. B. Kilgore, *Phys. Rev. Lett.* **88**, 201801 (2002), URL <https://link.aps.org/doi/10.1103/PhysRevLett.88.201801>.
- [33] M. Ciccolini, A. Denner, and S. Dittmaier, *Phys. Rev. D* **77**, 013002 (2008), 0710.4749.
- [34] J. Baglio, F. Campanario, S. Glaus, M. Mühlleitner, M. Spira, and J. Streicher, *Eur. Phys. J. C* **79**, 459 (2019), 1811.05692.
- [35] T. Schmidt and M. Spira, *Phys. Rev. D* **93**, 014022 (2016), 1509.00195.